Nonlinear Model-Based Control of an Experimental Reverse-Osmosis Water Desalination System

Alex R. Bartman, Panagiotis D. Christofides, and Yoram Cohen*

Department of Chemical and Biomolecular Engineering, University of California, Los Angeles, California 90095

This work focuses on the design and implementation of a nonlinear model-based control system on an experimental reverse-osmosis (RO) membrane water desalination system to address large set-point changes and variations in feedwater salinity. A dynamic nonlinear lumped-parameter model is derived using first-principles, and its parameters are computed from experimental data to minimize the error between model predictions and experimental RO system response. This model then is used as the basis for the design of a nonlinear control system, using geometric control techniques. The nonlinear control system is implemented on the experimental RO system, and its set-point tracking and disturbance rejection capabilities are successfully evaluated.

1. Introduction

Reverse-osmosis (RO) membrane desalination has emerged as one of the leading methods for water desalination, because of the low cost and energy efficiency of the process.[1] The lack of fresh water sources has necessitated further development of these desalination plants, especially in areas with dry climates. Even with advances in RO membrane technology, maintaining the desired process conditions is essential to successfully operating a RO desalination system. Seasonal, monthly, or even daily changes in feedwater quality can drastically alter the conditions in the RO membrane modules, leading to decreased water production, suboptimal system performance, or even permanent membrane damage.

To account for the variability of feedwater quality, a robust process control strategy is necessary. In a modern RO plant, automation and reliability are elements crucial to providing personnel safety, achieving product water quality, meeting environmental constraints, and satisfying economic demands. Industrial RO desalination processes primarily use traditional proportional and proportional−integral (PI) control to monitor production flow and adjust feed pumps accordingly.[2] While such control strategies are able to maintain a consistent product water (permeate) flow rate, they may fail to provide an optimal closed-loop response, with respect to set-point transitions, because of the presence of nonlinear process behavior.[3,4] In some cases, permeate production can decrease, because of scaling or fouling on the membrane surface. When this occurs, traditional control algorithms force the feed pumps to increase the feed flow rate, leading to an increased rate of scaling, irreversible membrane damage, and eventual plant shutdown. Traditional process control schemes are also unable to monitor plant energy usage and make adjustments toward energy-optimal operation.

Model-based control is a promising alternative to traditional RO plant control strategies. Several model-based methods, such as model-predictive control (MPC) and Lyapunov-based control, have been evaluated via computer simulations for use in RO desalination.[5−7,13] Experimental system identification and MPC applications can also be found in the literature.[8,9] Model-based control methods have also been used in conjunction with fault detection and isolation schemes to improve robustness of control methods in the presence of sensor and actuator failures.[6] Other automatic control methods utilize model-based control based on a linear model;[10] using step tests to create a model that is a linear approximation around the desired operating point. Several other traditional control methods have also been studied in the context of RO system integration with renewable energy sources.[11,12]

Motivated by the previously mentioned considerations, the goal of this work is to evaluate the effectiveness of a feedback linearizing nonlinear model-based controller through application to an experimental RO desalination system. A RO desalination system model is first derived based on mass and energy balances.[14] The parameters of the model are then computed based on experimental data gathered from the experimental RO desalination system, to minimize the error between model and experimental system responses. This dynamic nonlinear model is then used to derive a nonlinear feedback linearizing controller to conduct set-point transitions of the retentate flow rate by adjusting an actuated retentate valve. Efficient operation of the retentate valve (and, in turn, of the retentate stream flow rate/velocity) is integral to a RO system, because it (along with the feed pump speed) controls the clean water production rate and percentage of feedwater, which must be disposed of as waste. The nonlinear model-based controller is then implemented on the experimental system where it is shown to possess excellent set-point tracking and disturbance rejection capabilities. The nonlinear controller is also shown to outperform a PI control system.

2. RO System Model

In this section, a fundamental model of a representative RO desalination system is developed including all of the basic elements present in UCLA's experimental RO desalination system. In this system, shown in Figure 1, water enters the feed pump, which is equipped with a variable frequency drive (VFD), and is pressurized to the feed pressure (P_{sys}). The pressurized stream enters the membrane module, where it is separated into a low-salinity product (or permeate) stream with velocity v_p, and a high-salinity brine (or retentate) stream with velocity v_r. In the model, the individual spiral-wound membranes in series are assumed to be one large spiral-wound membrane in one large vessel, where any effects of individual membrane vessel interconnections are neglected. The pressures downstream of

* To whom correspondence should be addressed. E-mail address: pdc@seas.ucla.edu.

10.1021/ie900322x CCC: $40.75
Published on Web 04/17/2009

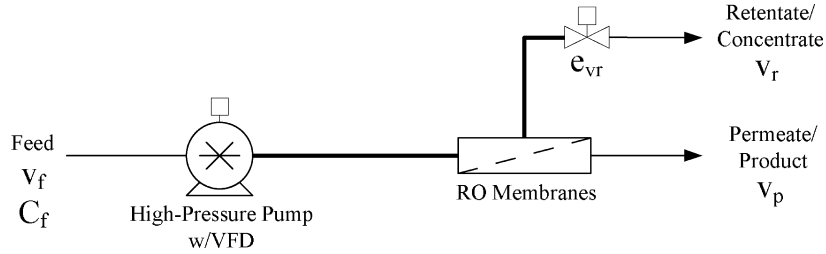

Figure 1. Reverse-osmosis (RO) system used for model development.

the actuated valve and at the permeate outlet are assumed to be equal to atmospheric pressure.

The model is based on a mass balance taken around the entire system and an energy balance taken around the actuated retentate valve (see ref 15 for more details on model development). In the model derivation, it is assumed that the water is an incompressible fluid, all components are operated on the same plane (so potential energy terms due to gravity can be neglected), and the density of the water is constant. It is also assumed that the effective concentration in the membrane module is a weighted average of the feed concentration and the brine stream concentration (see eq 6 below). The model derivation results in a nonlinear ordinary differential equation (ODE) for the retentate stream velocity and an algebraic relation for the system pressure. This model is an adaptation of a model developed in our previous work used to describe a similar RO desalination system.[15] In the previous work, the system utilized a feed pump with a constant feed flow rate but used a separate bypass stream with an actuated valve to control the velocity of the water feeding to the membrane units. An equation for the osmotic pressure based on effective concentration and temperature in the membrane unit was also developed in ref 16 and is used as an estimate in the model. Specifically, an energy balance is first taken around the retentate valve, which leads to the following differential equation:

$$\frac{dv_r}{dt} = \frac{P_{sys}A_p}{\rho V} - \frac{1}{2}\left(\frac{A_p e_{vr} v_r^2}{V}\right) \tag{1}$$

where v_r is the retentate stream velocity, P_{sys} the system pressure, A_p the cross-sectional area of the pipe, ρ the fluid density, V the system volume, and e_{vr} the retentate valve resistance. To compute an expression for the system pressure, in terms of the other process variables, an overall steady-state mass balance is taken to yield

$$0 = v_f - v_r - v_p \tag{2}$$

where v_f is the feed stream velocity and v_p is the permeate stream velocity. To get an expression for the system pressure, the following classical expression is used for the computation of the permeate stream velocity:

$$v_p = \frac{A_m K_m}{\rho A_p}(P_{sys} - \Delta\pi) \tag{3}$$

where A_m is the membrane area, K_m is the membrane overall mass transfer coefficient, and $\Delta\pi$ is the difference in osmotic pressure between the feed side of the membrane and the permeate side. Substituting eq 3 into eq 2, the following expression for the system pressure (P_{sys}) is obtained:

$$P_{sys} = \frac{\rho A_p}{A_m K_m}(v_f - v_r) + \Delta\pi \tag{4}$$

where the osmotic pressure ($\Delta\pi$) and effective average concentration at the membrane surface (C_{eff}) on the feed side can be computed from the following relations:

$$\Delta\pi = \delta C_{eff}(T + 273) \tag{5}$$

$$C_{eff} = C_f\left\{a + (1 - a)\left[(1 - R) + R\left(\frac{v_f}{v_r}\right)\right]\right\} \tag{6}$$

where C_f is the amount of total dissolved solids (TDS) in the feed, a is an effective concentration weighting coefficient, δ is a constant relating effective concentration to osmotic pressure, T is the water temperature (in degrees Celsius), and R is the fractional salt rejection of the membrane. Substituting eq 4 into the energy balance equation of eq 1 yields the following nonlinear ODE for the dynamics of the retentate stream velocity:

$$\frac{dv_r}{dt} = \frac{A_p^{\,2}}{A_m K_m V}(v_f - v_r) + \left(\frac{A_p}{\rho V}\right)\Delta\pi - \frac{1}{2}\left(\frac{A_p e_{vr} v_r^2}{V}\right) \tag{7}$$

Using the aforementioned dynamic equation, various control techniques can be applied using the valve resistance value (e_{vr}) as the manipulated input. As the valve resistance goes to zero, the valve behaves as an open pipe; as the valve resistance approaches infinity, the valve behaves as a total obstruction and the flow velocity goes to zero.[17]

To model the valve dynamics accurately, and to relate the experimental results to the concept of valve resistance value (e_{vr}), the concept of valve C_v is used. The definition of C_v for a valve in a water system is

$$C_v = \frac{Q_r}{\sqrt{P_{sys}}} \tag{8}$$

where Q_r is the volumetric flow rate ($Q_r = A_p v_r$) through the retentate valve. To obtain an expression for C_v, as a function of the retentate valve resistance (e_{vr}), we consider the steady-state form of the energy balance of eq 1, solve the resulting equation for P_{sys} and substitute the resulting expression for P_{sys} into eq 8 to yield

$$C_v = \frac{A_p}{\sqrt{(1/2)\rho e_{vr}}} \tag{9}$$

Depending on the type of valve and its flow characteristics, it is assumed that the C_v values (and, in turn, the e_{vr} values) can be related to the valve position (percentage open) through the following empirical logarithmic relation, based on commercially available valve data:[7]

$$O_p = \mu' \ln\left(\frac{A_p}{\sqrt{(1/2)\rho e_{vr}}}\right) + \varphi' \tag{10}$$

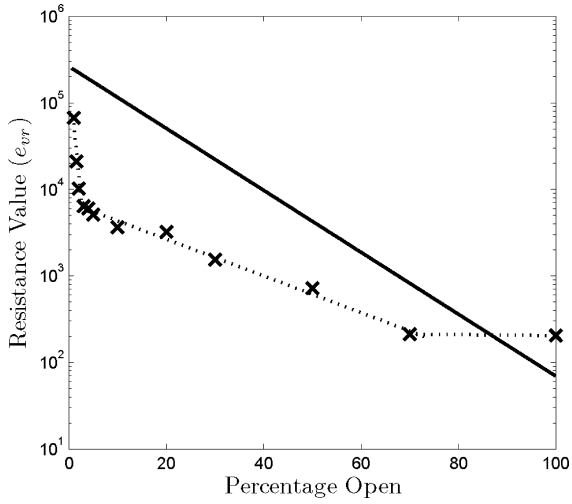

Figure 2. Correlation between valve resistance (e_{vr}) and the valve percentage open (O_p) value. Solid line (—) represents commercial theoretical data, crosses (×) represent experimentally measured data, and dashed lines (- - -) represent curve fittings to experimental data, using eqs 12−14.

Consolidating the constants and utilizing the properties of the natural logarithm, this expression can be simplified as

$$O_p = \mu \ln e_{vr} + \varphi \tag{11}$$

where μ and ϕ are constants that are dependent on the valve properties. The values of μ and ϕ for this model are taken from a paper based on the same experimental system at UCLA.[7] For the model presented in this paper, the curve relating valve position (O_p) to resistance value (e_{vr}) is shown in Figure 2. This figure shows that, as the valve position goes to zero (fully closed), the valve resistance values begin to grow at an increasing rate; in addition, as the valve approaches the fully open position, the resistance values change slowly. The data from the experimental system are also plotted on the figure, and it can be observed that the data does not fit the same logarithmic relation as the ideal valve curve. With respect to the accuracy of the sensors measurements of Figure 2, the error bars corresponding to these measurements have been computed and are on the order of the markers used to denote the data points; thus, they have not been included in Figure 2. Because of the shape of the experimental data curve, the data are fit in three segments with curve fits following a form similar to that of the theoretical curve. The first curve fit is applied to valve resistance values of $e_{vr} \approx 205-212$ and takes the form

$$O_p = -84.428 \ln(e_{vr}) + 459.21 \tag{12}$$

For $e_{vr} \approx 212-6200$, O_p is computed by

$$O_p = -2.0473 \ln(e_{vr}) + 18.141 \tag{13}$$

whereas, for $e_{vr} > 6200$, O_p is computed by

$$O_p = -0.0778 \ln(e_{vr}) + 0.9476 \tag{14}$$

This treatment of the valve characteristics allows for conversion of the experimental values of O_p to e_{vr} values in the model-based nonlinear control algorithm, and allows for e_{vr} values generated by the control algorithm to be translated to O_p values to be sent to the actuated valve on the experimental system. Capturing the nonlinearity present in the valve is extremely crucial when applying the control algorithms to the experimental system.

Table 1. Process Model Parameters Based on Experimental System Data

parameter	value
ρ	1007 kg/m^3
V	0.6 m^3
A_p	0.000127 m^2
A_m	15.6 m^2
K_m	6.4×10^{-9} s/m
C_f	4842 mg/L
a	0.5
T	22 °C
R	0.97

2.1. Computation of Nonlinear Model Parameters Based on Experimental Data. Most of the parameters of the model of eqs 7−14, such as the membrane area (A_m), water density (ρ), cross-sectional area of the pipe (A_p), and system volume (V) have constant values that can be obtained from the experimental system. Another key model parameter, the overall mass-transfer coefficient (K_m) was computed to match the model response to experimental step-test data. Specifically, K_m was computed using steady-state data from the experimental system by minimizing the difference between the model steady state and the experimental system steady state for various step tests. The computed values of K_m were then averaged to determine the best value for use in the model used for controller design. The values of the model parameters can be found in Table 1.

3. Control Algorithms

Two separate control loops are present in the control problem formulation. The first loop regulates the system pressure by adjusting the variable frequency drive speed (S_{VFD}) directly (effectively changing the feed flow rate). This control loop will be termed "loop I". In each set of experiments presented below, a proportional−integral (PI) feedback controller is used to keep the system pressure (P_{sys}) at the set-point value (P_{sys}^{sp}) of 150 psi. This control algorithm takes the form

$$S_{VFD} = K_f(P_{sys}^{sp} - P_{sys}) + \frac{K_f}{\tau_f}\int_0^{t_c}(P_{sys}^{sp} - P_{sys})\,dt \tag{15}$$

where S_{VFD} is the control action applied to the VFD speeds, K_f the proportional gain, and τ_f the integral time constant.

The second control loop (termed "loop II") uses a nonlinear model-based controller (for the purposes of comparison, P and PI controllers are also used in loop II). The nonlinear controller utilizes the error between the retentate velocity and its corresponding set point, but it also takes into account many additional system variables.[18−20] Specifically, the nonlinear model-based controller manipulates the actuated retentate valve position using measurements of the feed flow velocity (v_f), feed salinity (C_f), and retentate flow velocity (v_r). The nonlinear controller is designed following a feedback linearization approach. To derive the controller formula, the following linear, first-order response in the closed-loop system between v_r and v_r^{sp} is requested:

$$\frac{dv_r}{dt} = \frac{1}{\gamma}(v_r^{sp} - v_r) \tag{16}$$

Note that a first-order response is requested, because the relative degree between v_r and e_{vr} is one.[20] Using this approach, the following formula is obtained for the nonlinear controller:

$$e_{vr} = \frac{\frac{1}{\gamma}(v_r^{sp} - v_r) - \frac{A_p{}^2}{A_m K_m V}(v_f - v_r) - \frac{A_p \delta (T + 273)}{\rho V} C_{eff}}{\frac{-A_p}{2V}(v_r{}^2)} \quad (17)$$

To achieve offset-less response, integral action is added to the controller in eq 17 and the resulting controller takes the form

$$e_{vr} = \frac{\frac{1}{\gamma}(v_r^{sp} - v_r) + \frac{1}{\tau_{NL}}\int_0^{t_c}(v_r^{sp} - v_r)\,dt}{\frac{-A_p}{2V}(v_r{}^2)} + \frac{-\frac{A_p{}^2}{A_m K_m V}(v_f - v_r) - \frac{A_p \delta (T + 273)}{\rho V} C_{eff}}{\frac{-A_p}{2V}(v_r{}^2)} \quad (18)$$

As a baseline, the performance of the nonlinear controller is compared to a traditional form of control (P or PI, depending on the form of the nonlinear controller). Loop II, using P or PI control, uses the retentate (or concentrate) stream flow velocity to manipulate the actuated valve, to regulate the retentate stream velocity/flow rate. Under P or PI control, the control system for loop II takes the form(s):

$$O_p = K_r(Q_r^{sp} - Q_r) \quad (19)$$

or

$$O_p = K_r(Q_r^{sp} - Q_r) + \frac{K_r}{\tau_r}\int_0^{t_c}(Q_r^{sp} - Q_r)\,dt \quad (20)$$

where Q_r is the retentate stream volumetric flow rate and Q_r^{sp} is the retentate stream flow rate setpoint.

In each set of experiments, the performance of the nonlinear controller implemented on the experimental system is compared to the performance of the nonlinear controller implemented on the process model and to the performance of a P or PI controller implemented on the experimental system. These loops are diagrammed in Figures 3 and 4. The control algorithms were programmed into the data acquisition and control software to operate in real time with a sampling time of 0.1 s. In addition, the actuated retentate valve is powered by an electric motor with a maximum operating speed, which must be taken into account when attempting to simulate the nonlinear controller action. From testing on the experimental system, it was found that the actuated valve could travel its entire range within ~45 s; this provides an important constraint on the speed of valve opening/closing in the simulations of the form:

$$\left|\frac{dO_p}{dt}\right| \leq 2.22\ \%/s \quad (21)$$

To derive the constraint of eq 21, it is assumed that the valve speed is independent of valve position (the valve always turns at maximum speed). This is a physical constraint that is intrinsically taken into account in the experimental results and is programmed into the nonlinear model-based controller simulation as well (to facilitate comparison). In addition, when using the experimental system, the valve position is not allowed to fall under 1%, and any values sent to the valve above 100% are translated to the maximum value of 100% open. The lower constraint (>1%) is enforced so that the system pressure will not increase too rapidly. A constraint is also placed on the VFD to avoid pressure spikes (a maximum VFD speed of 4.5/10 is used). In the experiments presented in this work, the actuators do not reach these constraints.

4. Experimental System Description

The experimental reverse-osmosis (RO) water desalination system constructed at UCLA's Water Technology Research (WaTeR) Center was used to conduct the control experiments. This experimental system is comprised of a feed tank, two low-pressure feed pumps in parallel (which provide enough pressure to pass the feedwater through a series of cartridge filters while also providing sufficient pressure for operation of the high-pressure pumps), two high-pressure pumps in parallel (each capable of delivering ~4.3 gpm (gallons per minute) at 1000 psi), and a bank of 18 pressure vessels that contained Filmtec spiral-wound RO membranes. The high-pressure pumps are outfitted with variable frequency (or variable speed) drives that enable the control system to adjust the feed flow rate, using a 0−10 V output signal. The bank of 18 membranes are arranged into three sets of six membranes in series; in addition, for the control experiments presented below, only one bank of six membrane units was used. The experimental system uses solenoid valves controlled by the data acquisition and control hardware to enable switching between multiple arrangements of the membrane modules (two banks of six in parallel to one bank of six in series, or any number of the modules in series), while also allowing for control of the flow direction through the membrane banks. After the membrane banks, an actuated valve is present to control the cross-flow velocity (v_r) in the membrane units, while also influencing system pressure. This valve is used as an actuator for the control system utilizing the control algorithms presented in section 3. The resulting permeate and retentate streams are currently fed back into the tank in an overall recycle mode; however, for field operation, the system can be operated in a one-pass fashion.

The experimental system also has an extensive sensor and data acquisition network; flow rates and stream conductivities are available in real time for the feed stream, retentate stream, and permeate stream. The pressures ahead of each high-pressure pump, as well as the pressures before and after the membrane units (feed pressure and retentate pressure), are also measured. The system also includes sensors for measuring feed pH, permeate pH, in-tank turbidity, and feed turbidity after filtration (in real time). A centralized data acquisition system takes all of the sensor outputs (0−5 V, 0−10 V, 4−20 mA) and converts them to process variable values on the local (and web-accessible) user interface, where the control system is implemented. The data are logged into a local computer as well as onto a network database, where the data can be accessed via the Internet, while the control portion of the web-based user interface is only available to persons with proper authorization. The data acquisition and control system uses National Instruments software and hardware to collect the data at a sampling rate of 10 Hz and perform the necessary control calculations needed for the computation of the control action to be implemented by the control actuators. A photograph of the system can be seen in Figure 5.

5. Experimental Closed-Loop Results

In the control experiments presented in this paper, the experimental system was turned on and the PI loop that controlled the VFDs (loop I) was activated to bring the system

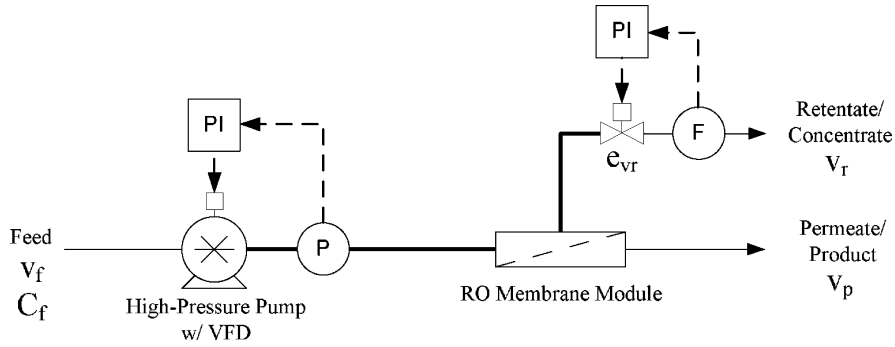

Figure 3. Reverse-osmosis (RO) system under two proportional−integral (PI) control systems: square symbols indicate PI controllers and circular symbols indicate measurement sensors (pressure (P), flow (F)).

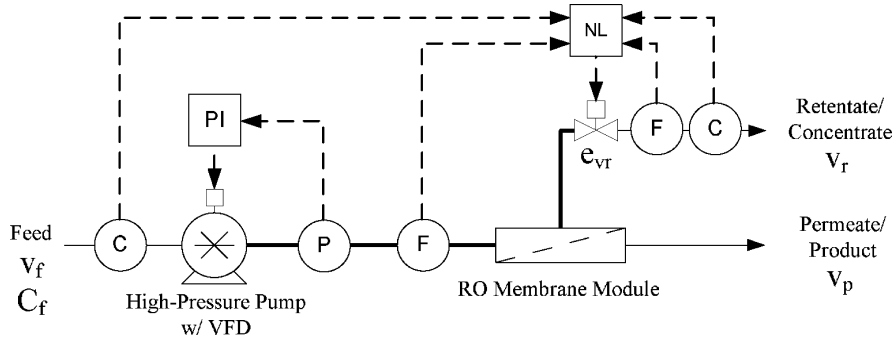

Figure 4. Reverse-osmosis (RO) system under proportional−integral (PI) control adjusting the variable frequency drive (VFD) speed and nonlinear control adjusting retentate valve position: square symbols indicate PI control and nonlinear control (NL) and circular symbols indicate measurement sensors (conductivity (C), pressure (P), flow (F)).

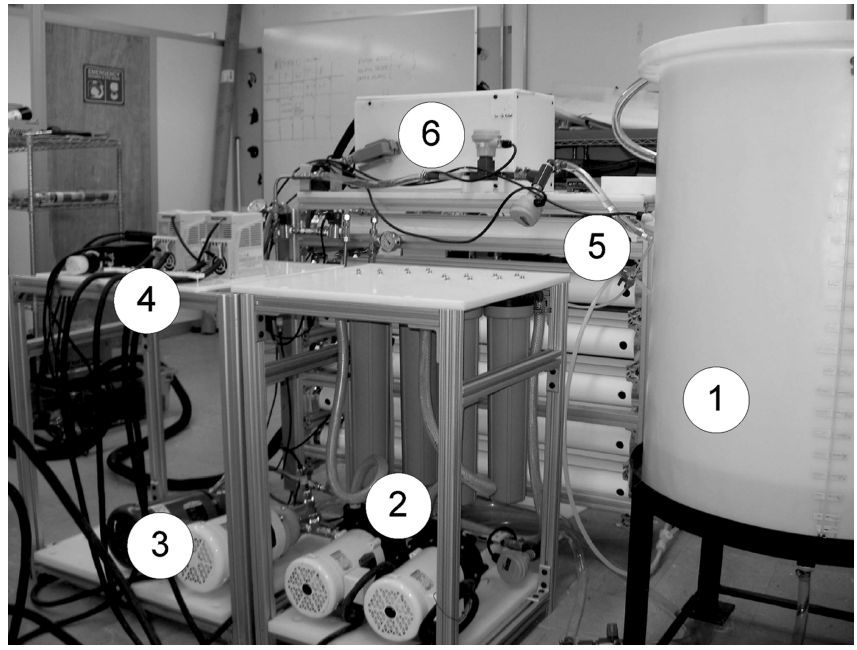

Figure 5. UCLA experimental RO membrane water desalination system. Legend: (1) feed tank, (2) low-pressure pumps and prefiltration, (3) high-pressure positive displacement pumps, (4) variable frequency drives (VFDs), (5) pressure vessels containing spiral-wound membrane units (three sets of six membranes in series), and (6) National Instruments data acquisition hardware and various sensors.

pressure to a setpoint of $P_{sys} = 150$ psi. The retentate flow rate was set to 1.5 gpm. After the system had been operating at this steady state for a sufficient period of time, loop II was activated to manipulate the retentate valve. All data taken from the experimental system were averaged (after the experiments), using a 19-point moving average to remove most of the measurement noise. The following sets of experiments compare the performance of the nonlinear controller with the performance of the P and PI controllers. The closed-loop response observed for the nonlinear controller applied to the dynamic process model is used as a baseline for comparison of controller performance, as well as to determine an approximate range of controller tunings for the experimental system.

In the first set of experiments, the retentate flow rate setpoint (interchangeable with the retentate velocity setpoint, $Q_r^{sp} = \upsilon_r^{sp} A_p$) was changed from 1.5 gpm to 3 gpm, while loop I is maintained

Table 2. Loop I PI Controller Tuning Parameters for the First Set of Experiments

parameter	value
K_f	0.01
τ_f	0.1
K_f^{sim}	0.01
τ_f^{sim}	0.1

Table 3. Loop II Controller Tuning Parameters for the First Set of Experiments (Parameters for Both Proportional and Nonlinear Controllers)

parameter	value
K_r	1
γ	0.6
γ^{sim}	0.6

at a pressure setpoint of 150 psi. In these experiments, the closed-loop performance of the nonlinear controller (without integral action) implemented on the experimental system is first evaluated against the performance of the simulated nonlinear controller (using the derived process model) and the performance of an experimentally implemented P controller. The feed salt concentration for the first set of experiments was ∼5400 ppm of sodium chloride (NaCl). The tuning parameters for the controllers can be found in Tables 2 and 3. Both loops were tuned (in the simulation and the experimental system) to achieve a slightly underdamped closed-loop output response (i.e., fastest approach to the steady state with minimal oscillatory output response).[21,22]

The results of the experiments were recorded using the data acquisition and control interface and are plotted in Figures 6−9. In Figure 6, it can be seen that the simulated model-based nonlinear controller yields a closed-loop response that converges the fastest to the steady state and achieves the smallest offset of any of the controllers. This result is expected, because the simulated controller is not subject to any type of plant−model mismatch or any measurement noise. The P controller implemented on the experimental system shows a significant offset (∼20% from the setpoint) and also demonstrates sustained oscillations after it levels off. These fairly large oscillations in retentate flow rate (caused by oscillations in the valve position)

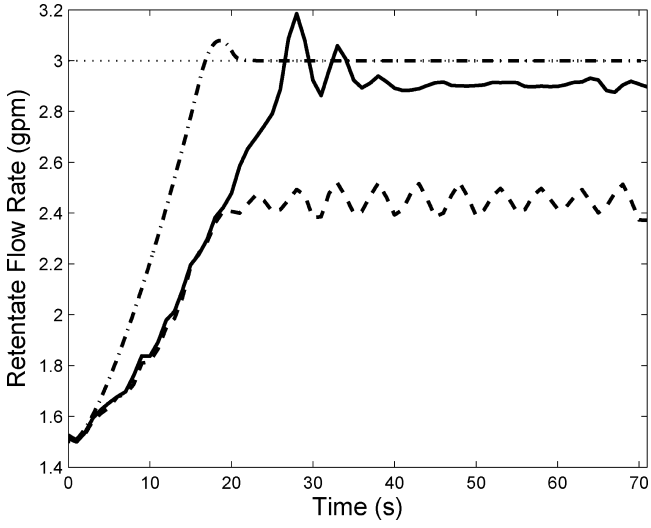

Figure 6. Profiles of retentate flow rate (Q_r), with respect to time, for retentate flow rate set-point transition from 1.5 gpm to 3 gpm under (- - -) proportional control, (—) nonlinear model-based control, and (- • - • -) nonlinear model-based control implemented via simulation on the process model. The horizontal dotted line denotes the retentate flow rate setpoint (Q_r^{sp} = 3 gpm).

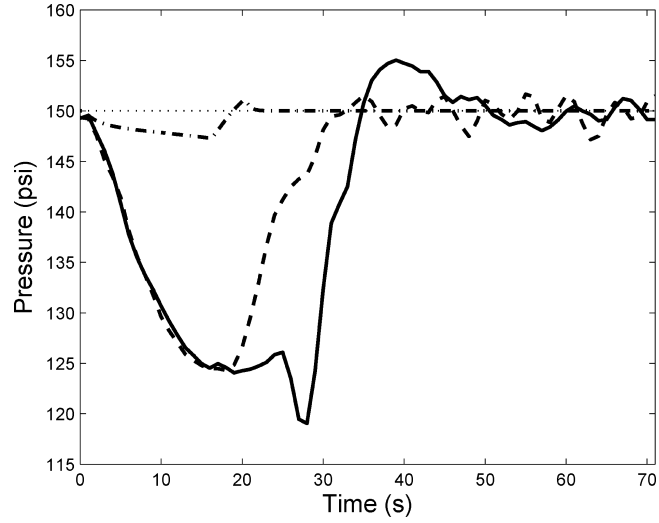

Figure 7. Profiles of system pressure (P_{sys}), with respect to time, for retentate flow rate set-point transition from 1.5 gpm to 3 gpm under (- - -) proportional control, (—) nonlinear model-based control, and (- • - • -) nonlinear model-based control implemented via simulation on the process model. The horizontal dotted line denotes the system pressure setpoint (P_{sys}^{sp} = 150 psi).

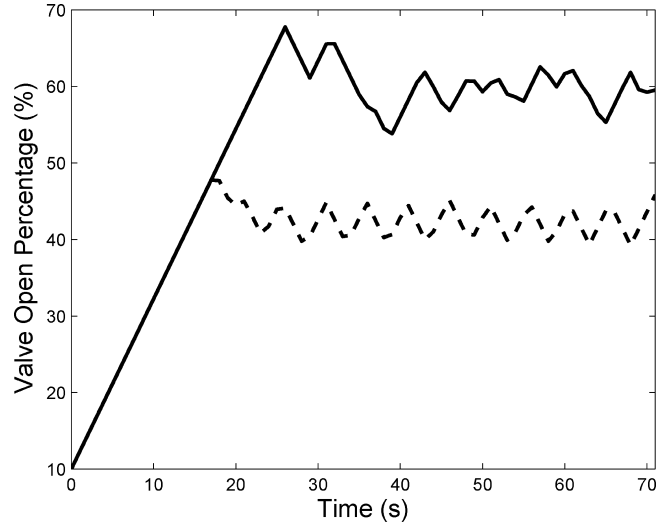

Figure 8. Profiles of valve open percentage (O_p), with respect to time, for retentate flow rate set-point transition from 1.5 gpm to 3 gpm (- - -) under proportional control and (—) nonlinear model-based control.

also lead to oscillations in the system pressure. These oscillations in the system pressure result in oscillations in the pump speed (from loop I) and can be detrimental to the operating life of the pumps. The nonlinear model-based controller (when applied to the experimental system) is shown to have a much smaller offset than the P controller in the same set-point tracking experiment (∼3%−4% from the setpoint). Brief oscillations are observed as the controller slightly overshoots the setpoint, but these oscillations decay and the system quickly stabilizes at the new setpoint. The smoothness of the closed-loop response under nonlinear control is due to the fact that it takes into account the action of loop I in the computation of the control action, while the P controller neglects the highly coupled nature of the two control loops. As the valve opens to allow for more flow through the retentate line (as dictated by the P controller), the system pressure decreases, causing loop I to increase the feed flow rate to maintain the system pressure at the setpoint. As a result of this, the retentate flow rate increases, forcing the P controller acting on the retentate valve to begin closing the valve. This

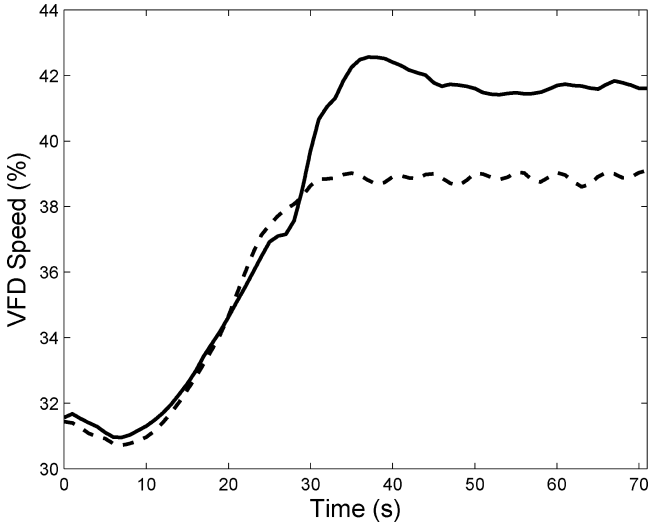

Figure 9. Profiles of variable frequency drive speed (S_{VFD}), with respect to time, for retentate flow rate set-point transition from 1.5 gpm to 3 gpm (- - -) under proportional control and (—) nonlinear model-based control.

interplay between the controllers causes the observed oscillations and can result in an increased time to reach the desired setpoint. Figure 7 shows that the simulated nonlinear controller demonstrates the smallest deviation from the system pressure setpoint (again, this result is expected, because the simulation is not subject to plant−model mismatch or measurement noise). Comparing the performance of the P controller and of the nonlinear controller when they are applied to the experimental system, it can be seen that the system response under the nonlinear controller deviates slightly more than under the P controller (∼5 psi in each direction), but the closed-loop pressure under the P controller demonstrates sustained periodic oscillations.

When examining the valve movement in Figure 8, it can be seen that each of the controllers has an equal initial slope, because of the maximum valve rate of the opening/closing constraint (eq 21). The nonlinear controller opens the valve to a greater extent than the P controller, leading to a smaller offset (larger retentate flow rate with higher valve position). The VFD input profiles in Figure 9 show that, because of the larger valve position value requested by the nonlinear controller, the VFD must accelerate slightly to achieve the same system pressure. When comparing the performance of the nonlinear controller to the performance of the P controller for retentate set-point changes (in Figure 6), it can be seen that, even though the nonlinear controller causes slightly greater fluctuations in system pressure, the offset from the setpoint is much smaller, and the oscillations are minimized.

In the second set of experiments, the retentate flow rate setpoint was changed from an initial value of 1.5 gpm to a new value of 0.8 gpm, while the VFD control loop is again maintained at a pressure setpoint of 150 psi. In this set of experiments, the performance of the nonlinear controller with integral term is evaluated against the performance of a PI controller (both of these controllers are implemented experimentally), and the performance of the nonlinear controller with integral action applied to the dynamic process model via simulations. The feed salt concentration for these experiments was ∼8200 ppm of NaCl. The tuning parameters for the controllers in this set of experiments can be found in Tables 4 and 5.

The results for the second set of experiments are plotted in Figures 10−13. Results for an alternate PI controller tuning are also presented in Figures 14−17. This alternate tuning was

Table 4. Loop I PI Controller Tuning Parameters for Second Set of Experiments

parameter	value
K_f	0.01
τ_f	0.1
K_f^{sim}	0.0091
τ_f^{sim}	0.1

Table 5. Loop II Controller Tuning Parameters for Second Set of Experiments (Parameters for Both PI and Nonlinear Controllers)

parameter	value
K_r	1
τ_r	(see captions)
γ	0.6
τ_{NL}	10
γ^{sim}	0.6
τ_{NL}^{sim}	10

presented to demonstrate the limited applicability of PI control to this system under a range of integral time constants.

Figure 10 shows that all of the closed-loop results (simulated and experimental) decrease at the same rate initially (due to the valve opening/closing rate constraint). As expected, the simulated nonlinear model-based controller with an integral term immediately converges to the setpoint with no offset, because it is not subject to any plant−model mismatch or measurement noise. As it is evident in Table 4, the integral time constant for the simulated controller is slightly different ($\tau_f = 0.01$, $\tau_f^{sim} = 0.0091$). The simulations where the nonlinear controller was applied to the process model were used to find an approximate range of controller parameters, but these values were implemented on the experimental system and changed slightly to achieve better closed-loop performance in the presence of plant−model mismatch. The speed of the closed-loop response under the nonlinear controller applied to the experimental system is slower, in terms of convergence to the setpoint, than that of the simulated case and the retentate flow rate reaches the setpoint within ∼145 s. The PI controller with $\tau_r = 5$ leads to an extremely slow convergence to the setpoint (on the order of 10 min). In Figure 14, a PI controller with the same gain K_r but with $\tau_r = 0.7$ is used to demonstrate the other extreme. This PI

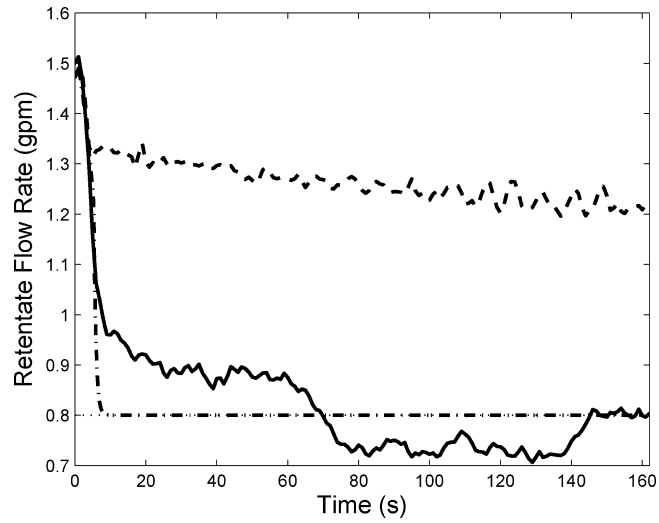

Figure 10. Profiles of retentate flow rate (Q_r), with respect to time, for retentate flow rate set-point transition from 1.5 gpm to 0.8 gpm under (- - -) proportional−integral control with $\tau_r = 5$, (—) nonlinear model-based control with integral action, and (- • - • -) nonlinear model-based control with integral action implemented via simulation on the process model. The horizontal dotted line denotes the retentate flow rate setpoint ($Q_r^{sp} = 0.8$ gpm).

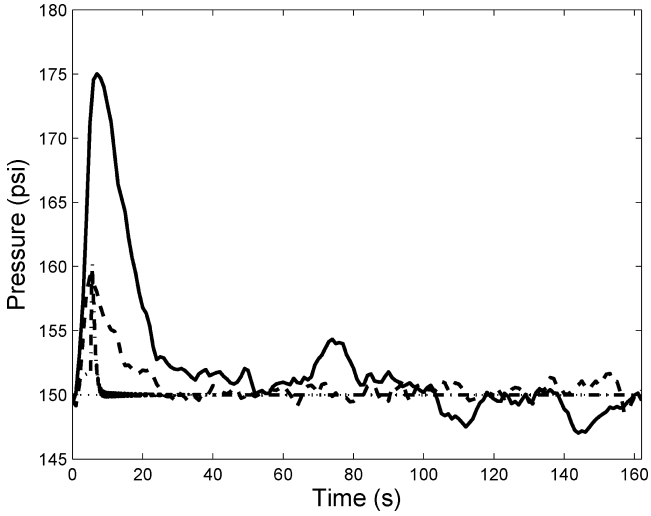

Figure 11. Profiles of system pressure (P_{sys}), with respect to time, for retentate flow rate set-point transition from 1.5 gpm to 0.8 gpm under (- - -) proportional−integral control with $\tau_r = 5$, (—) nonlinear model-based control with integral action, and (- • - • -) nonlinear model-based control with integral action implemented via simulation on the process model. The horizontal dotted line denotes the system pressure setpoint ($P_{sys}^{sp} = 150$ psi).

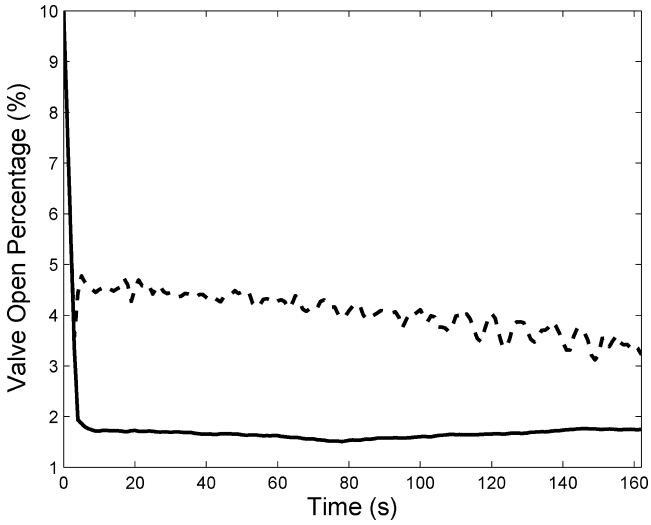

Figure 12. Profiles of valve open percentage (O_p), with respect to time, for retentate flow rate set-point transition from 1.5 gpm to 0.8 gpm under (- - -) proportional−integral control with $\tau_r = 5$ and (—) nonlinear model-based control with integral action.

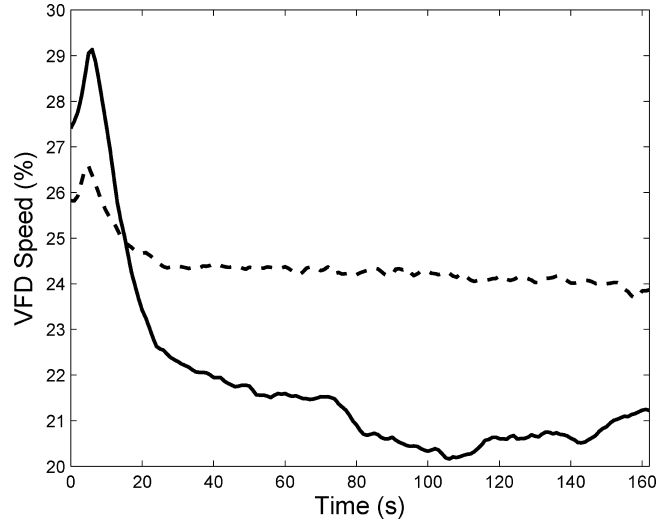

Figure 13. Profiles of variable frequency drive speed (S_{VFD}), with respect to time, for retentate flow rate set-point transition from 1.5 gpm to 0.8 gpm under (- - -) proportional−integral control with $\tau_r = 5$ and (—) nonlinear model-based control with integral action.

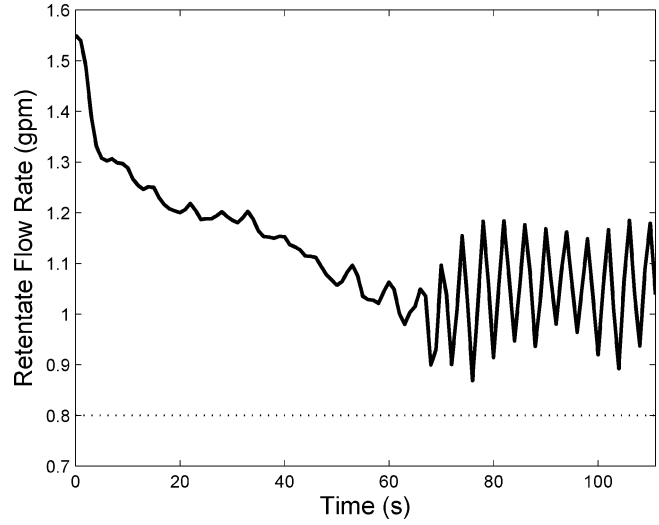

Figure 14. Profile of retentate flow rate, with respect to time, for retentate flow rate set-point transition from 1.5 gpm to 0.8 gpm under proportional−integral control ($\tau_r = 0.7$). The horizontal dotted line denotes the retentate flow rate setpoint ($Q_r^{sp} = 0.8$ gpm).

controller leads to a closed-loop response that converges to the setpoint at a faster rate than the PI controller with $\tau_r = 5$; however, as it can be seen, it results in significant oscillations around the setpoint, because of the coupling between the two control loops. These oscillations cause large fluctuations in the feed flow rate (due to the VFD control loop) and could damage the feed pumps and cause fatigue on system components.

Similar results are evident in Figure 11. The application of the nonlinear controller to the experimental system causes the most deviation from the pressure setpoint, because of the speed at which it converges to the setpoint. It can be seen that the PI controller causes almost no deviation from the setpoint (approximately the same as the simulated nonlinear controller), because the convergence (change in valve position) is much slower. As the valve closes, it causes the system pressure to rise, forcing loop I to take action to keep the system pressure at the setpoint. Slower valve actions allow more time for loop I to act and keep the system pressure at the setpoint, such as that in the case of the PI control with $\tau_r = 5$. When looking at the case of the PI controller where $\tau_r = 0.7$ (Figure 15), it can be seen that the initial pressure spike is much larger than in the case where $\tau_r = 5$, but smaller than that under the nonlinear controller.

It can be seen that a similar explanation applies in Figure 12, when looking at the valve positions for the various controllers. Specifically, it is observed that the valve position in the case of PI control (for both cases: $\tau_r = 5$ and $\tau_r = 0.7$ in Figure 16) is much more erratic and results in oscillations. From the results in the second set of experiments, it is again observed that the nonlinear controller achieves quick set-point transition with no offset (due to the addition of the integral term), while minimizing oscillations to a higher degree than the PI controllers. The S_{VFD} profiles show a trend similar to that in the first set of experiments (Figure 13); because of the fact that the valve position value is smaller for the nonlinear controller, the VFD speed slows down to maintain the set-point system pressure.

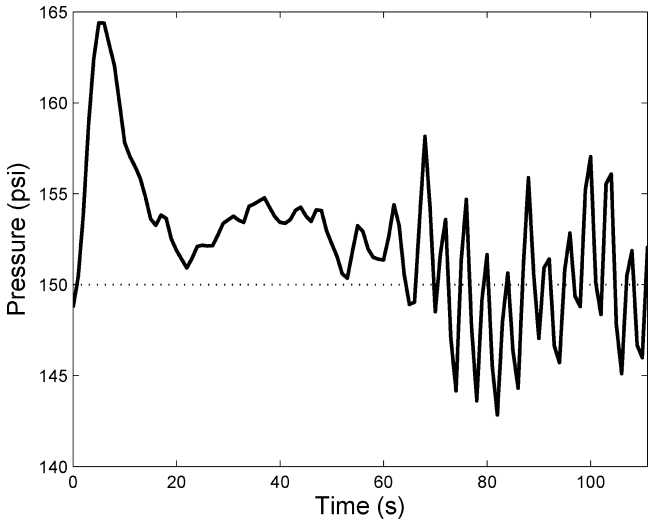

Figure 15. Profile of system pressure (P_{sys}), with respect to time, for retentate flow rate set-point transition from 1.5 gpm to 0.8 gpm under proportional−integral control ($\tau_r = 0.7$). The horizontal dotted line denotes the system pressure setpoint ($P_{sys}^{sp} = 150$ psi).

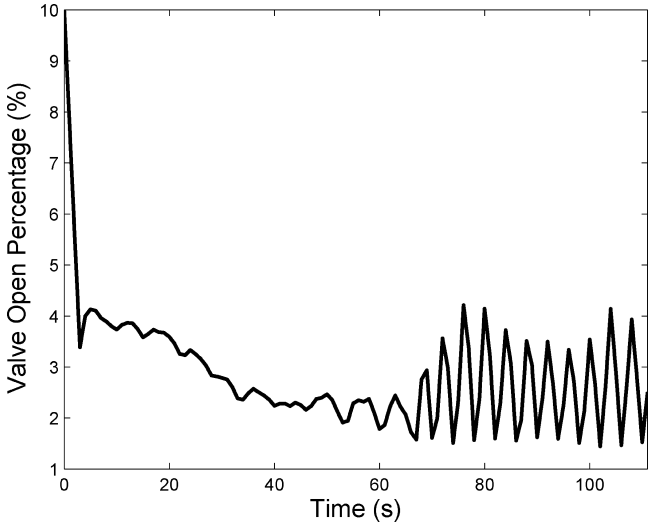

Figure 16. Profile of valve open percentage (O_p), with respect to time, for retentate flow rate set-point transition from 1.5 gpm to 0.8 gpm under proportional−integral control ($\tau_r = 0.7$).

As described in the Introduction, the variability of feedwater quality is also an important issue when designing controllers for RO systems. Although the time scales of feedwater quality variation are usually quite large (hours, days, or even weeks), the third set of experiments was designed to test the robustness of the controller when presented with a large change in feedwater quality on a smaller time scale (on the order of 10−30 s). The control parameters used in these experiments are shown in Tables 6 and 7. As in the first two sets of experiments, the retentate flow rate setpoint was 1.5 gpm, and the system pressure setpoint was 150 psi. Two relatively large pulses of sodium chloride (NaCl) were added to the system while it was operating under nonlinear model-based control with integral action. The feed concentration over the course of the experiment can be seen in Figure 18. The first pulse of salt was added at ∼90 s, bringing the feed conductivity from 5500 μS up to a final value of near 7000 μS. The second pulse was added after the feed salinity stabilized and brought the feed conductivity up to a final value of ∼8000 μS (after mixing). The effects of these pulses

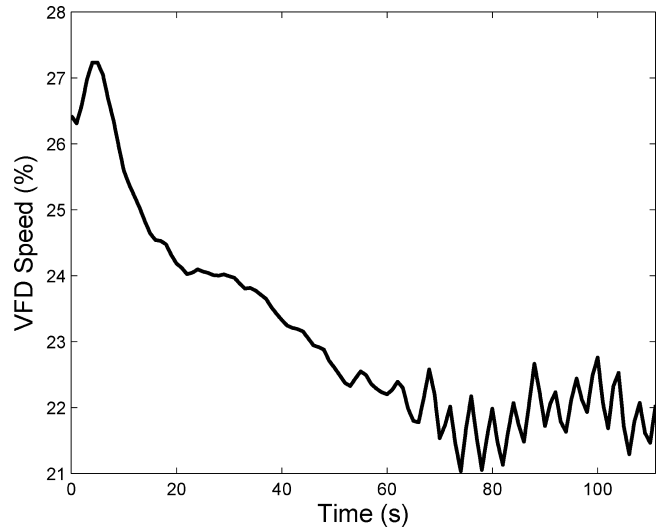

Figure 17. Profile of variable frequency drive speed (S_{VFD}), with respect to time, for retentate flow rate set-point transition from 1.5 gpm to 0.8 gpm under proportional−integral control ($\tau_r = 0.7$).

Table 6. Loop I PI Controller Tuning Parameters for Feed Disturbance Experiments

parameter	value
K_f	0.01
τ_f	0.1

Table 7. Loop II Controller Tuning Parameters for Feed Disturbance Experiments

parameter	value
γ	0.6
τ_{NL}	10

on valve position, retentate flow rate, and system pressure can be seen in Figures 19−22.

Figure 19 shows that, through all of the feed salt concentration changes, the nonlinear model-based controller keeps the retentate flow rate within 2%−3% of the set-point value of 1.5 gpm. Figure 20 also demonstrates that the control system is able to keep the system pressure within similar bounds from the set-point value of 150 psi. When examining the control action in Figure 21, it can be seen that the valve closes slowly. Specifically, as the feed concentration increases, the osmotic

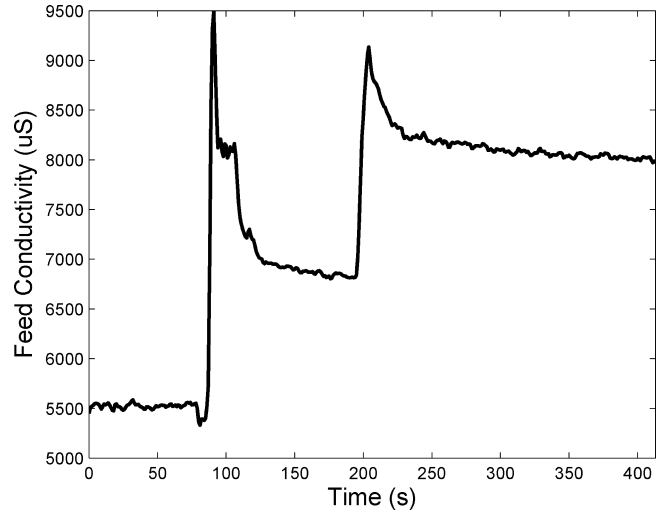

Figure 18. Profile of feed conductivity, with respect to time; disturbance rejection experiment under nonlinear control with integral action.

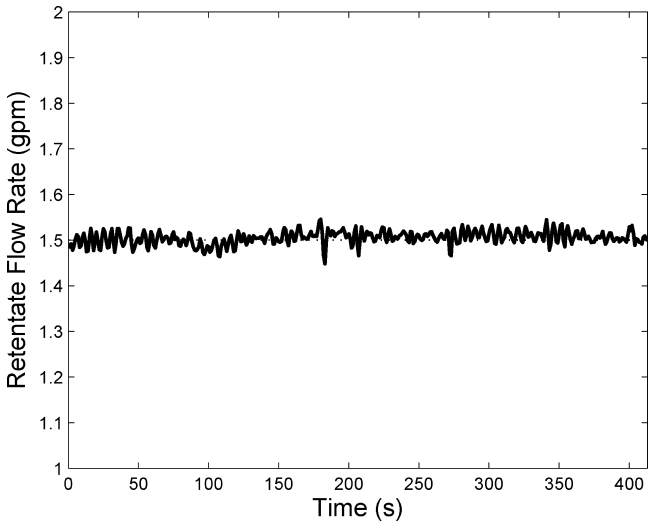

Figure 19. Profile of retentate flow rate, with respect to time; disturbance rejection experiment under nonlinear control with integral action (solid line). The horizontal dotted line is the retentate flow rate setpoint (1.5 gpm).

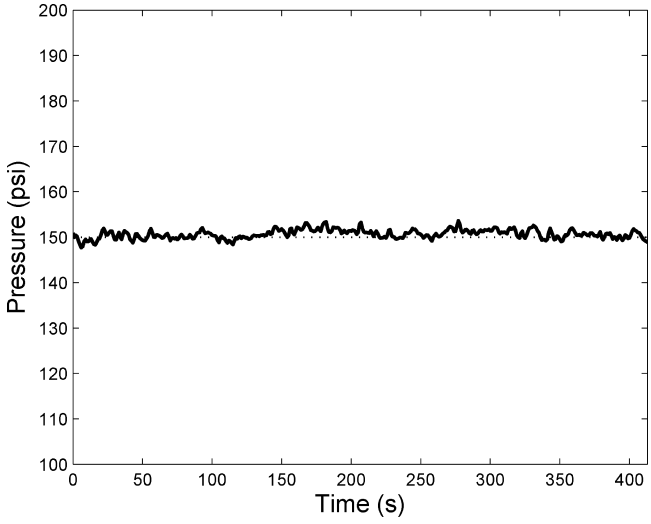

Figure 20. Profile of system pressure (P_{sys}), with respect to time; disturbance rejection experiment under nonlinear control with integral action (solid line). The horizontal dotted line is the pressure setpoint ($P_{sys}^{sp} = 150$ psi).

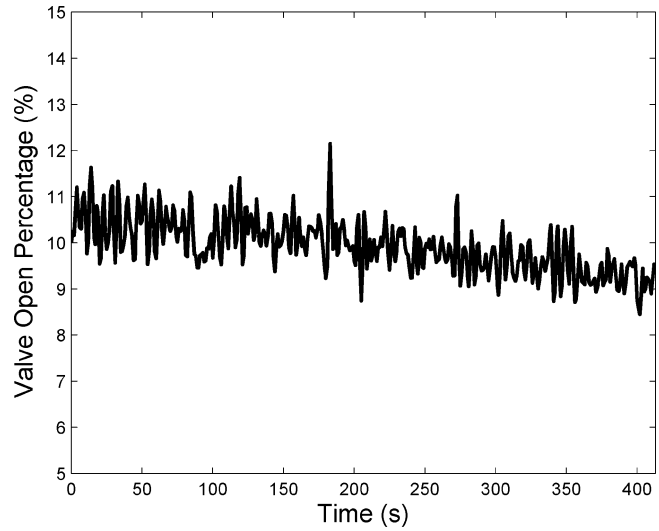

Figure 21. Profile of valve open percentage (O_p), with respect to time; disturbance rejection experiment under nonlinear control with integral action.

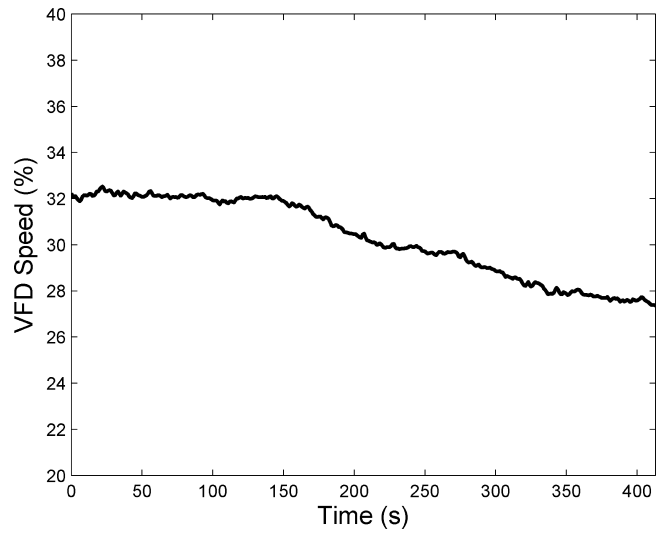

Figure 22. Profile of variable frequency drive speed (S_{VFD}), with respect to time; disturbance rejection experiment under nonlinear control with integral action.

pressure resisting flow through the membrane also increases. If the system pressure is kept constant, this forces a greater percentage of the water to remain in the concentrate stream (lower driving force through the membrane due to the osmotic pressure increase). Because the retentate stream is controlled at a setpoint of 1.5 gpm, the controller closes the actuated valve to mitigate this effect. When examining the S_{VFD} control action, it can be seen that S_{VFD} slowly decreases as the feed conductivity increases. This trend is reasonable, because the water that is entering the membrane units is facing more resistance, due to increased osmotic pressure across the membranes. This increase in osmotic pressure raises the system pressure for a fixed feed flow rate; therefore, the VFDs must slow the feed flow rate to maintain the set-point system pressure. Again, the nonlinear controller is shown to perform very well in the presence of feed salt concentration variability. Also note that the size of the moving average window (1.9 s) is small enough to reduce most of the measurement noise, but it is also small when compared to the transient system response time. The disturbance rejection experiment also shows that, when a large change in salinity occurs in a short time, the system reaches steady state again on the order of 100 s. In an industrial RO system, the feedwater salinity will change much slower, on the order of minutes, hours, or even days.

6. Conclusions

In this work, a nonlinear model-based control strategy was developed and experimentally implemented on a reverse-osmosis (RO) membrane water desalination system. First, a dynamic fundamental model that describes the RO desalination system was derived; the parameters of this model were then computed using step test data from UCLA's experimental reverse-osmosis desalination system. Specifically, correlations were derived to relate the actuator position to model parameters, and the remaining model parameters were computed based on the experimental data. A nonlinear model-based control algorithm was then designed based on the constructed process model. This nonlinear controller was implemented to manipulate the retentate stream actuated valve, along with a proportional−integral controller that was used to manipulate the variable frequency drive speed, adjusting the feed flow rate. The performance of

the nonlinear controller was compared to the performance of proportional and proportional−integral control algorithms, as well as benchmarked against the simulated nonlinear model-based controller during retentate flow rate set-point transitions. It was demonstrated that the nonlinear controller is much better suited to address the highly coupled system dynamics during set-point transitions and was shown to outperform the traditional control schemes. The model-based nonlinear controller also performed well when the experimental RO system was subjected to a series of large step changes in feed salt concentration. Our future research plans in this direction will focus on (a) networked control implementation, so that medium-scale RO desalination processes can be operated in a remote fashion, and (b) networked monitoring issues, to be able to facilitate detection and isolation of control actuator/measurement sensor/control system faults.

Acknowledgment

Financial support from the State of California Department of Water Resources is gratefully acknowledged.

Literature Cited

(1) Rahardianto, A.; Gao, J.; Gabelich, C. J.; Williams, M. D.; Cohen, Y. High recovery membrane desalting of low-salinity brackish water: Integration of accelerated precipitation softening with membrane RO. *J. Membr. Sci.* **2007**, *289*, 123–137.

(2) Alatiqi, I.; Ettourney, H.; El-Dessouky, H. Process control in water desalination industry: An overview. *Desalination* **1999**, *126*, 15–32.

(3) Aboabboud, M.; Elmasallati, S. Potable water production from seawater by the reverse osmosis technique in Libya. *Desalination* **2007**, *203*, 119–133.

(4) Chen, J.; Wang, F.; Meybeck, M.; He, D.; Xia, X.; Zhang, L. Spatial and temporal analysis of water chemistry records (1958−2000) in the Huanghe (Yellow River) basin. *Global Biogeochem. Cycles* **2005**, *19*, GB3016.

(5) Abbas, A. Model predictive control of a reverse osmosis desalination unit. *Desalination* **2006**, *194*, 268–280.

(6) McFall, C. W.; Bartman, A. R.; Christofides, P. D.; Cohen, Y. Control of a Reverse Osmosis Desalination Process at High Recovery. *Ind. Eng. Chem. Res.* **2008**, *47*, 6698–6710.

(7) Bartman, A. R.; McFall, C. W.; Christofides, P. D.; Cohen, Y. Model predictive control of feed flow reversal in a reverse osmosis desalination process. *J. Process Control* **2009**, *19*, 433–442.

(8) Assef, J. Z.; Watters, J. C.; Deshpande, P. B.; Alatiqi, I. M. Advanced control of a reverse osmosis desalination unit. *J. Process Control* **1997**, *4*, 283–289.

(9) Burden, A. C.; Deshpande, P. B.; Watters, J. C. Advanced control of a B-9 Permasep permeator desalination pilot plant. *Desalination* **2001**, *133*, 271–283.

(10) Alatiqi, I. M.; Ghabris, A. H.; Ebrahim, S. System identification and control of reverse osmosis desalination. *Desalination* **1989**, *75*, 119–140.

(11) Herold, D.; Neskakis, A. A small PV-driven reverse osmosis desalination plant on the island of Gran Canaria. *Desalination* **2001**, *137*, 285–292.

(12) Liu, C. K.; Park, J.; Migita, R.; Qin, G. Experiments of a prototype wind-driven reverse osmosis desalination system with feedback control. *Desalination* **2002**, *150*, 277–287.

(13) Gambier, A.; Badreddin, E. Application of hybrid modeling and control techniques to desalination plants. *Desalination* **2002**, *152*, 175–184.

(14) Dickson, J. M.; Spencer, J.; Costa, L. M. Dilute single and mixed solute systems in a spiral wound reverse osmosis module. Part I: Theoretical model development. *Desalination* **1992**, *89*, 63–88.

(15) McFall, C. W.; Christofides, P. D.; Cohen, Y.; Davis, J. F. Fault-Tolerant Control of a Reverse Osmosis Desalination Process. In *Proceedings of 8th IFAC Symposium on Dynamics and Control of Process Systems*, Cancun, Mexico, 2007; Vol. 3, pp 163−168.

(16) Lu, Y.; Hu, Y.; Zhang, X.; Wu, L.; Liu, Q. Optimum design of reverse osmosis system under different feed concentration and product specification. *J. Membr. Sci.* **2007**, *287*, 219–229.

(17) Bird, R. B.; Stewart, W. E.; Lightfoot, E. N. *Transport Phenomena*, Second Edition; John Wiley and Sons: New York, 2002.

(18) El-Farra, N. H.; Christofides, P. D. Integrating Robustness, Optimality, and Constraints in Control of Nonlinear Processes. *Chem. Eng. Sci.* **2001**, *56*, 1841–1868.

(19) El-Farra, N. H.; Christofides, P. D. Bounded Robust Control of Constrained Multivariable Nonlinear Processes. *Chem. Eng. Sci.* **2003**, *58*, 3025–3047.

(20) Christofides, P. D.; El-Farra, N. H. *Control of Nonlinear and Hybrid Process Systems: Designs for Uncertainty, Constraints and Time-Delays*; Springer: New York, 2005; 446 pp.

(21) Ogunnaike, B. A.; Ray, W. H. *Process Dynamics, Modeling, and Control*; Oxford University Press: New York, 1994.

(22) Riggs, J. B.; Karim, M. N. *Chemical and Bio-Process Control*, 3rd ed.; Ferret Publishing: Lubbock, TX, 2006 (ISBN 0-9669601-4-9).

Received for review February 25, 2009
Revised manuscript received March 6, 2009
Accepted March 11, 2009

IE900322X